



# Ascorbyl palmitate–PCL fiber mats loaded with strontium polyphosphate nanoparticles for guided bone regeneration

Bothaina M. Abdel-Hady<sup>1</sup> · Basma Ekram<sup>1</sup>  · Werner E. G. Müller<sup>2</sup> · Abdul Aziz M. Gad<sup>3</sup> · Xiaohong Wang<sup>2</sup> · Heinz C. Schröder<sup>2</sup> · Emad Tolba<sup>1</sup>

Received: 29 November 2022 / Revised: 15 May 2023 / Accepted: 25 May 2023 /

Published online: 7 June 2023

© The Author(s) 2023

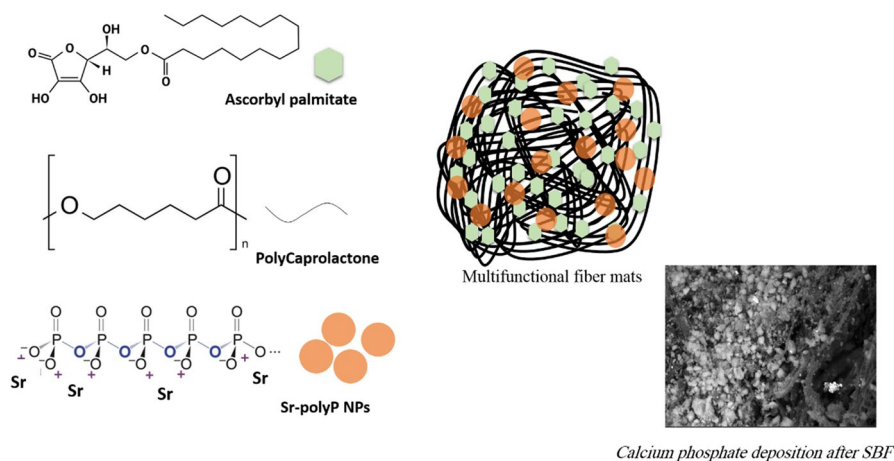
## Abstract

Multifunctional fiber mats are explored as potential bioactive matrices for the development of the next generation of guided bone regeneration membranes with tunable microstructure, strength and therapeutic activity. In the present study, polycaprolactone (PCL) nanofibers with different concentrations of ascorbic acid derivatives (ascorbyl palmitate) and strontium polyphosphate nanoparticles (Sr-polyP NPs) were fabricated. The obtained PCL mats scaffolds were assessed not only for microstructure structure features, including morphological observation, hydrophilicity and tensile strength, but also in *vitro* water uptake, biodegradation (under enzymatic and hydrolytic conditions), bioactivity using SBF, as well as ascorbic acid release study. The observed results showed that the mean fiber diameter of the PCL fibers ( $388 \pm 340$  nm) increased with the increase in the concentration of the ASP and Sr-polyP NPs. The addition of ascorbyl palmitate caused an increase in viscosity from  $40.6 \pm 2.5$  to  $66.6 \pm 2.0$  cP in the case of 20% AsP/PCL; however, it caused a decrease in conductivity from  $7.3 \pm 0.4$  to  $6.38$   $\mu$ s, while there was an obvious increase in the viscosity and conductivity by Sr-polyP Nps addition from  $40.6 \pm 2.5$  cP in the case of PCL only to  $88.3 \pm 2.5$  cP in the case of PA1/SP<sub>15</sub>. The contact angle decreases from  $125.9 \pm 2.5^\circ$  in the case of PCL only to  $112 \pm 4$  and  $102 \pm 2.4^\circ$  in the case of 20% loaded ascorbyl palmitate-PCL mats and 15% Sr/PCL, respectively. Moreover, the assessment of the antioxidant activity of PCL fiber mats containing 10% and 20% ascorbyl palmitate demonstrated that the 20% ascorbyl palmitate-PCL fiber mats have a higher antioxidant effectiveness compared to the 10% mats. This could be attributed to the controlled release of ascorbic acid from PCL, which occurs after 7 days. However, the highest tensile strength was observed for 5% Sr-polyP NPs-loaded PCL/AsP mats at  $1.52 \pm 0.51$  MPa. Further increase of Sr-polyP NPs content resulted in a clear decrease of tensile strength to  $1.13 \pm 0.13$  and  $0.93 \pm 0.71$  for 10% and 20% ascorbyl palmitate-PCL mats, respectively. Importantly, the fabricated AsP and Sr-polyP NPs-loaded PCL fiber mats showed induction of calcium phosphate deposition in SBF and the ability to sustain release of ascorbic acid over a time period of 28 d, in addition to the enhancement in cell

Extended author information available on the last page of the article

proliferation compared to PCL only suggesting their application as a favorable synthetic matrix to amplify guided bone regeneration process.

### Graphical abstract



**Keywords** Ascorbyl palmitate · Polycaprolactone · Strontium polyphosphate · Electrospinning · Guided bone regeneration · Drug release

### Introduction

Guided bone regeneration (GBR) has been boosted as a tremendous option in modern dentistry and orthopedic surgeries. The basic concept of GBR involves the use of a barrier membrane to simply direct the osseous regeneration by preventing the ingrowth of soft tissues into the defect area and thus, providing appropriate surrounds for the osteogenesis process [1, 2]. Indeed, GBR is clinically used to enhance the augmentation of alveolar ridge defects, improve the biological outcomes of bone graft materials, and even minimize the risk of dental/bone implant complications [3]. Current GBR membranes are typical of two types, non-resorbable membranes (such as expanded polytetrafluoroethylene (e-PTEF), high-density-PTFE membranes and titanium mesh) or resorbable membranes as collagen and synthetic polyesters (i.e. polyglycolides (PGAs), polylactides (PLAs), or their copolymers). Compared to non-resorbable membranes, resorbable membranes provide an ideal solution to avoid the second operation which is associated with non-resorbable ones [3, 4]. However, there are some drawbacks in the current GBR membranes including lack of tissue integration, low mechanical properties, proper degradation rate and poor ability to induce bone depositions [5]. The ideal GBR membrane should have a proper degradation rate in which it stays in its place with adequate mechanical properties for about 4–6 weeks to avoid connective tissues from growing into alveolar bone defects [6, 7].

Polymeric membranes/mats of the fibrous structure have been introduced as a functional structure to resemble the extracellular matrix and to facilitate cell adhesion, migration and proliferation [8]. Fibrous mats can be produced by different techniques including the phase separation technique [9], self-assembly [10] and template synthesis [11]. As a simple and alternative approach, electrospinning has been recalled to fabricate ultrafine polymer fibers of unique arrays and tunable physico-chemical features. The ability to handle a diverse array of products has been made possible by utilizing various electrospinning techniques such as basic solution electrospinning, blended electrospinning, coaxial electrospinning, emulsion electrospinning, melt electrospinning and gas jet electrospinning based on the specific requirements [12, 13].

Various polymerization methods have been used to produce eco-friendly, biocompatible, and biodegradable polyesters such as poly (hydroxyalkanoate) (PHA), poly (lactic acid) (PLA) and poly (caprolactone) (PCL) from petroleum-based feedstocks [14]. PCL is a FDA-approved synthetic polymer that has garnered significant attention for the development of green materials and biomaterials due to its favorable characteristics such as good processability, electrospinnability, biodegradability and miscibility [14]. As a result, PCL-based biomaterials have a wide range of applications in the biomedical field. However, the potential application of PCL material in bone tissue regeneration is limited and generally requires the incorporation of bioactive materials to promote bone regeneration and healing processes [15].

Polyphosphate (polyP) is the inorganic polymer of orthophosphate (Pi) that acts as a phosphate source in bone mineralization and as a metabolic energy generator in the extracellular space [16, 17]. The polyP is enzymatically hydrolyzed by the alkaline phosphatase enzyme (ALP), which breaks the phosphoanhydride bonds between phosphate groups [18]. Amorphous Calcium/polyP nanoparticles meet the fundamentals of being fully biocompatible beside facilitating tissue regeneration [16]. Strontium (Sr) has attracted interest due to its potential to promote the proliferation and differentiation of bone-forming cells and its inhibition of the resorbing activity of osteoclasts [19, 20]. In addition, it cannot only significantly increases the bioactivity of grafts and hasten the regeneration in the defect area, but can also improve angiogenesis *in vitro* and *in vivo* by increasing the proangiogenic factors [21, 22]. As previously reported by our group [23], Sr-polyP particles reveal excellent biological features for superior bone regeneration based on the obvious increase of mineral deposition and expression of ALP and BMP-2 in SaOS cells *in vitro*, as well as tissue healing *in vivo*.

Among many antioxidants used in medicine, L-ascorbic acid (Vitamin C) is one of the well-known powerful naturally occurring antioxidant that is able to block some of the damage caused by free radicals and serves as a co-factor in several metabolic activities, including the hydroxylation of proline and lysine residues in collagen, folding of pro-collagen and deposition as mature collagen [24, 25]. Nevertheless, ascorbic acid is not physiologically stable but is known to work more efficiently in aqueous media than in hydrophobic conditions [26]. The structure of ascorbic acid is made of a ring with several hydroxyl groups at positions 2, 3, 5 (secondary alcoholic residue) and 6 (primary alcoholic residue). The chemical modification of its hydroxyl groups would improve not only its stabilization as an antioxidant but

also would provide new derivatives with multiple physiological function properties for new biomedical applications. Ascorbyl palmitate (AsP) is an amphipathic derivative of ascorbic acid that has an antioxidant effect almost equal to ascorbic acid [27]. It showed more stability than ascorbic acid due to the presence of hydrophobic palmitate chains that can penetrate the cell more easily and have better capability to protect lipids and further cell components from free radical peroxidation [27, 28]. The current study aims to prepare and characterize nanofibrous PCL membranes with different concentrations of AsP and also different concentrations of Sr-polyP NPs and evaluate their optimum concentrations as well as their biocompatibility.

## Material and methods

### Materials

Sodium polyphosphate (Na-polyP) with an average chain length of 40 phosphate units was purchased from Chemische Fabrik Budenheim (Germany), 2,2 diphenyl 2 picryl hydrazyl hydrate (DPPH), and poly ( $\epsilon$ -caprolactone) purchased from Sigma-Aldrich (USA), Strontium chloride ( $\text{SrCl}_2 \cdot 6\text{H}_2\text{O}$ ), and Ascorpyl palmitate (6-O-palmitoyl-L-ascorbic acid) were purchased from Sigma-Aldrich (Germany).

### Preparation of Sr-polyP NPs

Sr-polyP NPs were fabricated using an analogous procedure as described by Müller et al. [23]. The preparation started with dissolving 1 g of sodium polyphosphate powder in 25 mL of distilled water. On the other side, 5.16 g of  $\text{SrCl}_2 \cdot 6\text{H}_2\text{O}$  salt was dissolved in 25 mL of distilled water. The strontium solution was then added dropwise to the polyP solution, keeping the pH at 10. The suspension formed was left overnight under stirring. The particles were collected by decantation, washed three times with ethanol and dried at 60 °C.

### Electrospinning of PCL/AsP and PCL/AsP/Sr-polyP fiber mats

A polymeric solution of 10% PCL in the solvent system (50:50 chloroform–methanol) was prepared as listed in Table 1 according to the method described by Eldurini et al. [29]. For ascorbic acid containing mats, ascorbyl palmitate was added at two different ratios to PCL until complete dissolution and then, the PCL was added. The Sr-polyP NPs at different concentrations of 5, 10 and 15% (wt/wt) of PCL were added to the solvent only and then, subjected to sonication for 1 h for complete dispersion. Then, the calculated amount of PCL was added to form a final concentration of 10% (wt/v). The prepared solutions were loaded into a syringe with a 21G needle with a tip to collector distance of 12 cm under 20 kV applied voltage using a Glassman High Voltage Series [30]. The solutions were electrospun at room temperature (about 25 °C) and relative humidity (RH) of  $50 \pm 2\%$ . The fibers were collected

**Table 1** Electrospun PCL fiber mats composition and their formulation

Formulation	AsP content (wt%)	Sr-polyP content (wt%)
P	0	0
PA1	10	0
PA2	20	0
PA1/SP <sub>5</sub>	10	5
PA1/SP <sub>10</sub>	10	10
PA1/SP <sub>15</sub>	10	15

in the form of a net fibrous mat (up to 3 mm in thickness). For solvent removal, the electrospun mats were vacuum dried at 40 °C for 3 h.

### Physicochemical characterization

Viscosity measurements were studied for all samples after a constant using Brookfield viscometer (Model DV-III Ultra). Each sample was put in the built-in stainless steel container attached to a temperature controller at 25 °C using a S21 spindle at 50 RPM [31]. The effect of adding different concentrations of AsP and Sr-polyP NPs on the conductivity of PCL solution was measured by using a conductivity meter (HC3010, Trans instruments) at 25 °C [32]. The morphology and fiber diameter were examined using a field emission Scanning Electron Microscope SEM (Jeol JXA 840, Japan). The mean fiber diameter of the samples was determined by measuring about 50 individual fibers using the image analysis software (Image J 1.42q software, NIH, Bethesda, Maryland, USA) [33]. Fourier-transform infrared (FTIR) spectroscopy was performed with an attenuated total reflectance-FTIR spectroscope/Varian IR spectrometer (Agilent, Santa Clara; CA). Surface hydrophilicity was estimated by determining the contact angle using a Compact video microscope (CVM), manufactured by SDL-UK, contact angle measured by a horizontal plate camera perpendicular to the liquid droplet plane. Thermal analysis (DSC/TGA) of the sample was tested using an SDTQ600 analyzer with a rate of 10 °C min<sup>-1</sup> under argon. The tensile strength of the electrospinning nanofibrous membranes was measured using Universal Testing Machine (Lloyd Instruments Ltd LR10 K, Hampshire, UK) at a stroke rate of 10 mm per minute. The samples were of dimensions of 10 mm width and 80 mm length with a gap length of 2 cm. The thickness of the mats was assessed using a digital Vernier Caliper. Each mat was repeated five times, and the results were averaged.

### In vitro study

#### Antioxidant assay

The antioxidant activity was determined using the radical scavenging activity of PCL mats loaded with AsP against 2,2 diphenyl 2 picryl hydrazyl hydrate (DPPH),

as described by Plank et al. [34]. The change in color of DPPH (from deep violet to light yellow) was measured at 517 nm on a UV–visible light spectrophotometer. The samples were kept in the absence of light for 15 min at room temperature, and the decrease in absorbance was measured. Each mat was repeated thrice. Radical scavenging activity was calculated by the following formula.

$$\% \text{ Inhibition} = [(A_B - A_A) / A_B] \times 100$$

where  $A_B$  = absorption of the blank sample ( $t=0$  min)  $A_A$  = absorption of test extract solution ( $t=15$  min).

The IC50 was calculated from the scavenging activities (%) versus concentrations of the respective sample curve.

### Degradation and water uptake

Degradation and water uptake assessments are done according to the method described by Deyab et al. [35]. The electrospun mats were cut and weighed into  $2 \times 1 \text{ cm}^2$  samples and was termed as initial weight ( $W_i$ ). Afterward, the samples were soaked into 15 ml of Phosphate Buffer Solution (PBS) and incubated at  $37^\circ \text{C}$  for 1, 3, 7, 14, 30 days. After each prescribed day, the mats were taken out and dried with a filter paper to absorb all the surface solution; then, the samples were then weighed, denoted wet weight ( $W_w$ ). The samples were weighed again after drying for 24 h at room temperature and this is termed the dry weight ( $W_d$ ). The percentage weight loss and the water uptake percentage were calculated according to the following relations (Kandil et al. [36]):

$$\text{Weight loss (\%)} = \frac{W_i - W_d}{W_i} \times 100 \quad (1)$$

$$\text{Water uptake (\%)} = \frac{W_w - W_i}{W_i} \times 100 \quad (2)$$

A degradation test was also performed in the presence of a lipase enzyme. The degradation medium was prepared by dissolving lipase enzyme at a final concentration of  $2 \text{ mg mL}^{-1}$  and 0.02% (wt/v) sodium azide as a bacteriostatic agent in a 0.05 M Tris–HCl buffer, pH 7.4. Three square samples were placed in sealed vials containing 3 ml of the degradation medium. The samples were incubated for different time intervals 3, 6 and 12 and 24 days. The lipase degradation medium was changed every three days. At each incubation period, the samples were slowly removed and dried at  $40^\circ \text{C}$  to determine dry weight after lipase degradation.

### Ascorbic acid content and release

The ascorbic acid release from the prepared PCL mats was estimated by UV–spectrophotometer as described by Avizheh et al. [37]. In brief, AsP-loaded PCL samples were incubated into Tris–HCl buffer in the presence and absence of lipase enzyme

(as mentioned in Sect. "Degradation and water uptake"). The released ascorbic acid was measured at a wavelength of 265 nm. The concentration of ascorbic acid in the investigated samples was calculated via calibration plot as the quantity in  $\mu\text{g/ml}$ . The release profiles were determined by calculating the concentrations of ascorbic acid in the Tris–HCl buffer over different time intervals.

### Bioactivity

Mats were cut into rectangular shapes with a dimension of  $2 \times 1 \text{ cm}^2$  and placed in a 15 ml centrifuge tube containing SBF solution and incubated for 28 days at  $37 \text{ }^\circ\text{C}$  to examine their ability for hydroxyapatite layer formation [38]. The hydroxyapatite layer formation is assessed by SEM [39].

### Cultivation of SaOS-2 cells

The human osteogenic sarcoma cells (SaOS-2) cells (Sigma #89050205) were cultured in McCoy's medium (Biochrom Seromed, Berlin, Germany) provided with 5% heat-inactivated fetal calf serum (FCS), 2 mM L-glutamine and gentamicin (50  $\mu\text{g/ml}$ ) in six-well plates (Sigma-Greiner) as described by Wiens et al. [40]. The cells were seeded at a density of  $2 \times 10^4$  cells per 3 ml well and cultivated for 3 d in medium/FCS.

### Cell proliferation/cell viability assay

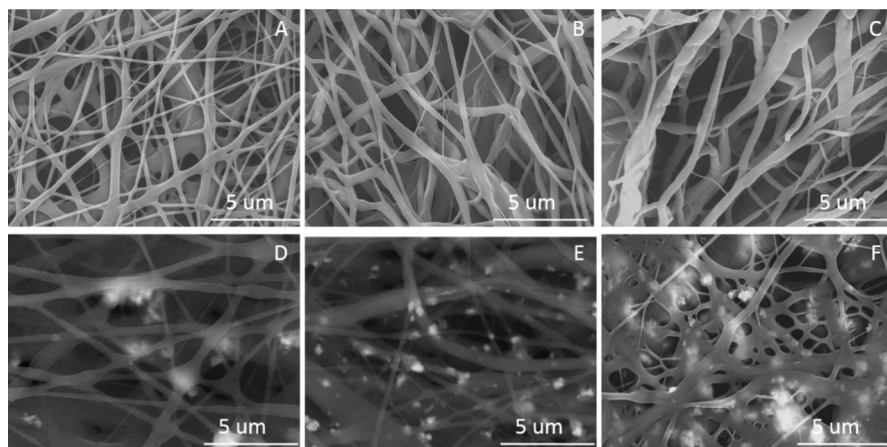
The mats were sterilized with 70% (v/v) ethanol aqueous solution for 20 min, then washed by PBS thrice, followed by exposure to ultraviolet radiation (280–315 nm UVB; 20  $\text{mJ/cm}^2$ ) for 1 h before cell culture experiments. The cytotoxicity was assessed by the colorimetric method, based on the oxidation of the tetrazolium salt. SaOS-2 cells were seeded into the 48-well plates and cultured for 3 d in McCoy's medium/15% FCS. Two parallel series of experiments were carried out. The cells were cultured either in the absence or in the presence of the mats. Then, after a 3 d incubation period, the cytotoxicity of the cells was assessed with 3-[4,5-dimethyl thiazole-2-yl]-2,5-diphenyl tetrazolium (MTT; #M2128, Sigma). Ten parallel experiments were performed as described by Müller et al. [30].

### Statistical analysis

The values reported are the average  $\pm$  standard deviations. Statistical analysis was performed with the one-way ANOVA test, attached by Excel software. Values of  $p < 0.05$  were considered statistically significant.

**Table 2** Change in viscosity, conductivity and fiber diameter of PCL samples

Sample name	Viscosity (cP)	Conductivity ( $\mu\text{s}$ )	Mean Fiber Diameter (nm)
P	$40.66 \pm 2.51$	$7.30 \pm 0.46$	$388 \pm 34$
PA1	$62.33 \pm 1.52$	$6.51 \pm 0.71$	$418 \pm 24$
PA2	$66.66 \pm 2.08$	$6.38 \pm 0.55$	$433 \pm 25$
PA1/SP <sub>5</sub>	$83.3 \pm 2.51$	$6.79 \pm 0.12$	$677 \pm 35$
PA1/SP <sub>10</sub>	$86.6 \pm 1.52$	$10.80 \pm 0.74$	$891 \pm 62$
PA1/SP <sub>15</sub>	$88.3 \pm 2.51$	$12.64 \pm 0.37$	$630 \pm 97$

**Fig. 1** SEM micrographs of PCL fiber mats and their fibers diameter distribution. **A** P, **B** PA1, **C** PA2, **D** PA1/SP<sub>5</sub>, **E** PA1/SP<sub>10</sub> and **F** PA1/SP<sub>15</sub>

## Results

### Fiber morphology

As shown in Table 2, there is an increase in the fiber diameter due to the increase of the solution viscosity with the addition of AsP and Sr-polyP NPs nanoparticles. On the other side, the conductivity measurements show a slight decrease with the addition of AsP and a remarkable increase with Sr-polyP NPs nanoparticles which could be attributed to the excess of free charges caused by the nanoparticles' addition. The morphology of the electrospun PCL fibers after the addition of AsP is shown in Fig. 1. The SEM observations reveal an increase in fiber diameter with increasing AsP content and a clear deformation of fiber morphology with increasing Sr-polyP NPs nanoparticles content. By increasing the Sr-polyP NPs nanoparticles content, the fibers begin to appear in a flattened shape due to the increase in viscosity and carrying ability of the polymeric fibers.



## Fourier transformed infrared

FTIR spectra for electrospun mats containing ascorbyl palmitate were shown in Fig. 2. The ascorbyl palmitate shows bands at  $2919\text{ cm}^{-1}$  and  $2850\text{ cm}^{-1}$  that are related to the C–H stretches and the carbonyl stretching band of lactones ring of ascorbic acid at  $1754\text{ cm}^{-1}$  and  $1728\text{ cm}^{-1}$ . The two bands at  $1667\text{ cm}^{-1}$  and  $1628\text{ cm}^{-1}$  are due to the C=C stretching vibrations. The spectrum of neat PCL electrospun fiber has shown two bands at  $2940\text{ cm}^{-1}$  and  $2868\text{ cm}^{-1}$  which are typical for the symmetric and asymmetric C–H stretching. The sharp band at  $1723\text{ cm}^{-1}$  belongs to the stretching vibrations of the ester-carbonyl groups (C=O). However, the bands for PCL were not shifted, and the intensity of the carbonyl group was changed with the addition of ascorbyl palmitate (AsP); this is also reported by Du and his coworkers in their investigation of this blend by XPS, and they showed that the peak at  $288.8\text{ eV}$  suggested an increase in the atomic percentages of the carbon atoms participating in C–O–C/C–OH of the ascorbic structure and also an increase in the peak area of the O-atoms, participating in C–O–C/C–OH bonds [41]. The FTIR spectra of the samples after Sr-polyP NPs addition are very close to the pure PCL spectrum and show only small new bands and some shifts. They all exhibit two bands at  $2940\text{ cm}^{-1}$  and  $2868\text{ cm}^{-1}$  which are typical for the symmetric and asymmetric C–H stretching of PCL. The sharp band at  $1723\text{ cm}^{-1}$  belongs to the stretching vibrations of the ester-carbonyl groups (C=O). By the addition of Sr-polyP NPs, a small new band related to Sr-polyP ascribed to a symmetric stretching of P–O–P at  $876\text{ cm}^{-1}$  and also small

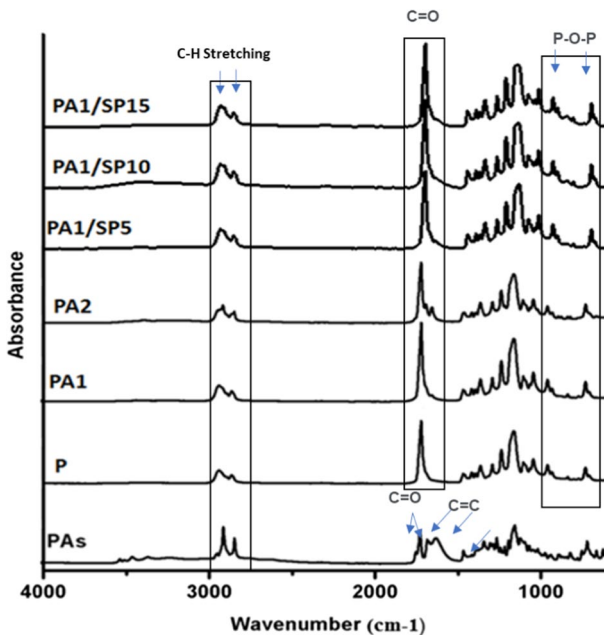


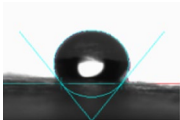
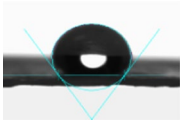
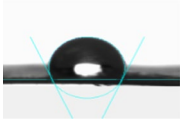
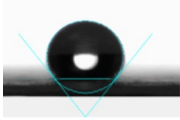
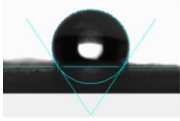
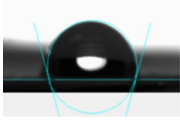
Fig. 2 FTIR spectra for the ascorbyl palmitate and the electrospun mats

new bands at  $995/986\text{ cm}^{-1}$  for the asymmetric and symmetric stretching of P–O–P. Moreover, the broad bands near  $3428\text{ cm}^{-1}$  are attributed to stretching vibrations of hydroxyl groups.

### Contact angle

The surface wettability of the samples is shown in Table 3. As the amount of AsP increases, the contact angle decreases due to the amphipathic nature of the AsP. The addition of Sr-polyP NPs caused a slight decrease in the hydrophobicity of PCL from  $125^\circ$  to  $104^\circ$  in the case of 15% Sr-polyP NPs due to the increase in surface charge. The results agree with the results obtained by Bayrak and his co-workers in their study of the addition of hydroxyapatite to PCL due to the increase of surface energy [42].

**Table 3** Contact angles of the different electrospun mats

Sample	Contact angle ( $^\circ$ )	Image
P	$125.9 \pm 2.57$	
PA1	$121 \pm 1.81$	
PA2	$112 \pm 5.14$	
PA1/SP <sub>5</sub>	$121.45 \pm 1.01$	
PA1/SP <sub>10</sub>	$120.13 \pm 1.76$	
PA1/SP <sub>15</sub>	$104.02 \pm 2.68$	

### Water uptake and degradation

Water uptake indicates the diffusion of nutrients and blood supply across the membrane. Analysis for water uptake measurements of the fabricated mats after 24 h indicates that both AsP and Sr-polyP NPs have significant effects on PCL’s water absorption behavior. The water uptake percentage of all the samples is shown in Fig. 2. As can be seen, the highest water uptake values were observed for PCL mats loaded with AsP followed by the PCL mats loaded with Sr-polyp compared to pure PCL mats. In addition, it is clearly seen that as the Sr-polyp NPs content increases, the amount of water uptake decreases. This can be related to the change in samples porosity due to the changes in fiber diameters and the agglomerations of Sr-polyp NPs, as indicated by SEM observation.

The degradation behavior of the different electrospun mats is also shown in Fig. 3. In general, the degradation of the PCL ester linkages in PBS occurs due to hydrolytic degradation [38]. However, the PCL mat demonstrated very high stability and low degradability. Considering the PCL/AsP samples a slight increase in degradation rate is detected which could be due to the release of ascorbic acid into the PBS. The increase of Sr-polyP NPs content increased the degradation rate of the electrospun PCL. The results agree with the results of Díaz and his coworkers in their study of the effect of nano-hydroxyapatite addition in the in-vitro degradation of PCL scaffolds [43].

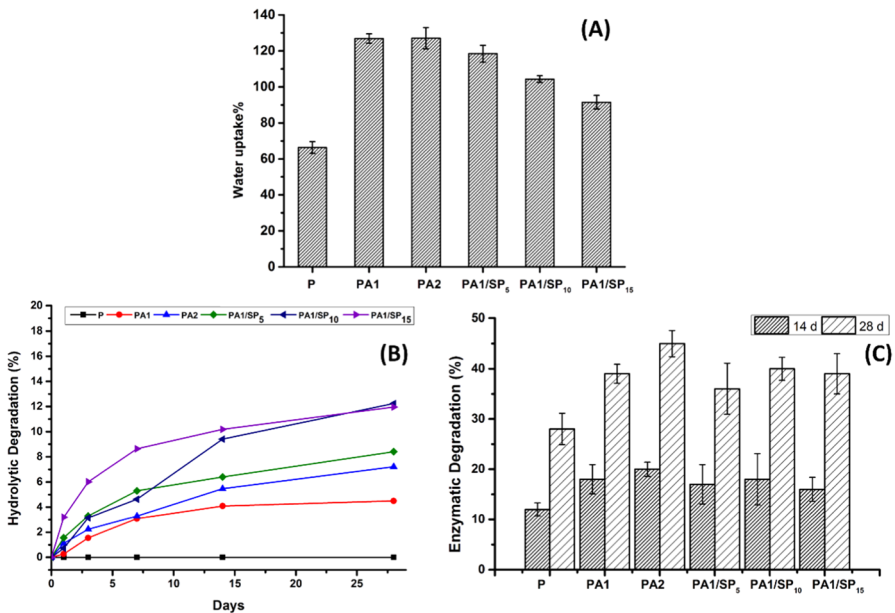


**Fig. 3** **a** The water uptake index of the electrospun mats, **b** the hydrolytic degradation percentage of the electrospun mats through 28 days and **c** the enzymatic degradation percentage of the electrospun mats through 28 days

Enzymatic degradation of PCL loaded with AsP and Sr-polyP was carried out at 37 °C in PBS solution containing lipase for 12 and 14 days, as shown in Fig. 4. The weight loss was increased with increasing AsP which indicates that lipase accelerates the AsP degradation. The results also demonstrate that the PCL mats loaded with Sr-polyP NPs show a lower weight loss which could be attributed to the decrease in water uptake, as previously mentioned.

### Effect of incubation time on ascorbic acid release

However, it was clearly observed that ascorbic acid was released under both conditions. The release of ascorbic acid was significantly increased in the presence of lipase. Under hydrolytic conditions, the PA1 sample releases about 25% and 58% of the total ascorbic acid content after 1 d and 28 d, while approximately 47.3% and 91% of the total ascorbic acid was released in the presence of lipase enzyme at the said time intervals. On the other hand, the PA1/SP mats showed a lower ascorbic acid release, in which an obvious difference was observed among the three samples with various Sr-polyP NPs content. For instance, one day AA release of PA1/SP mats under hydrolytic conditions was in the following order: 22.8% for PA1/SP<sub>5</sub> sample, 12.2% for PA1/SP<sub>10</sub> sample and 10.1 for PA1/SP<sub>15</sub> sample. The same was also observed in the presence of lipase enzyme (44.6%, 37.4% and 31.3% for PA1/SP<sub>5</sub>, PA1/SP<sub>10</sub> and PA1/SP<sub>15</sub> samples, respectively).

### Antioxidant assay

The antioxidant activity of palmitoyl ascorbic acid and PCL mats loaded with palmitoyl ascorbic acid were measured by the DPPH (2,2-diphenyl-1-picrylhydrazyl) assay. The results showed that the IC<sub>50</sub> of palmitoyl-L-ascorbic acid was (32 ± 4 nM). The IC<sub>50</sub> value reveals the antioxidant activity of mats. It is calculated as the concentration of antioxidants needed to decrease the initial DPPH

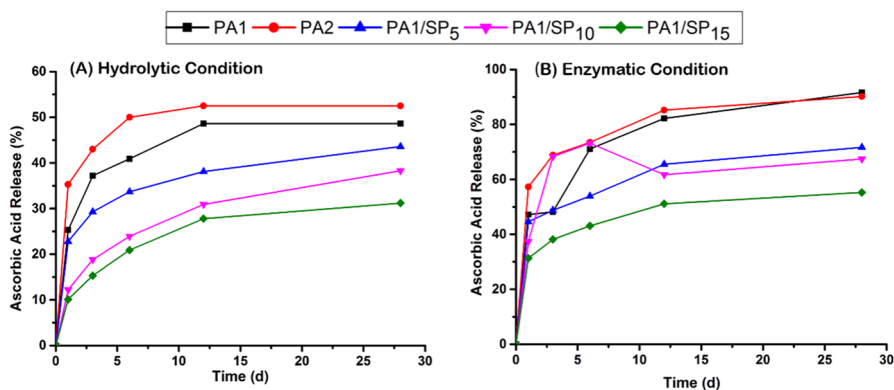


**Fig. 4** Effect of incubation time on releasing of ascorbic acid from AsP-loaded PCL fiber mats under a Hydrolytic condition and b Enzymatic conditions

concentration by 50% [44, 45]. Thus, the lower the  $IC_{50}$  value the higher the antioxidant activity.

The antioxidant activity of 10 and 20% ascorbyl palmitate–PCL fiber mats was measured by DPPH assay after 0.25, 3, 7, 10, 14 and 21 d, as shown in Fig. 5. The results indicate that the 20% is more efficient antioxidant than 10% ascorbyl palmitate–PCL fiber mats. The samples exhibit a stable antioxidant capability after 7 d in which the DPPH scavenging % was not slightly changed after 10, 14 and 21 d. This may be attributed to the controlled release of ascorbic acid from PCL that occurs after 7 d.

## Mechanical properties

The mechanical behavior of the samples is shown in Fig. 6. Incorporation of palmitoyl ascorbic showed an increase in the mechanical properties, but with increasing the concentration to 20% there is a decrease in the tensile strength. Ascorbyl palmitate addition causes the fiber to be smoother and hence lowers its mechanical properties. As a result, the mechanical properties of 10% As-PCL were shown to be better and hence, it was chosen for further studies. As shown in Table 4, the addition of Sr-polyP NPs slightly decreased the tensile strength from 1.21 MPa for neat PCL to 0.93 MPa for PA1/SP<sub>15</sub> and also decreased the elongation at break, but there is a slight increase in Young's modulus due to the hardness occurred due to the loading of the Sr-polyP NPs.

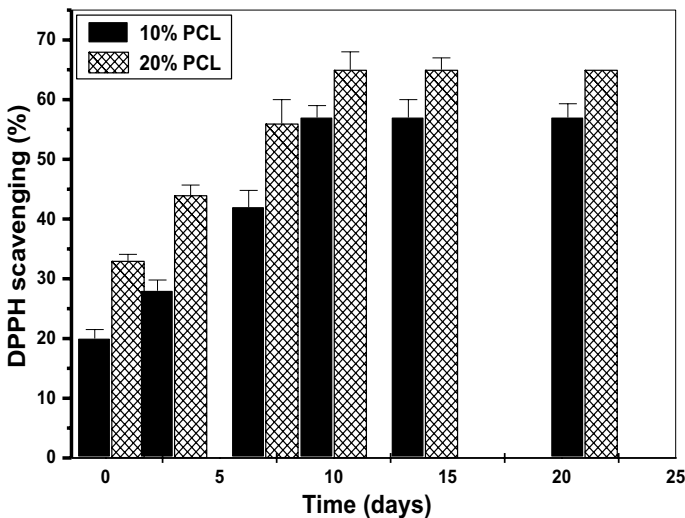


**Fig. 5** DPPH scavenging (%) for 10 and 20% ascorbyl palmitate–PCL fiber mats after different incubation time intervals. The antioxidant potential was calculated and expressed as mean values  $\pm$  SD for five experiments ( $p \leq 0.01$ )

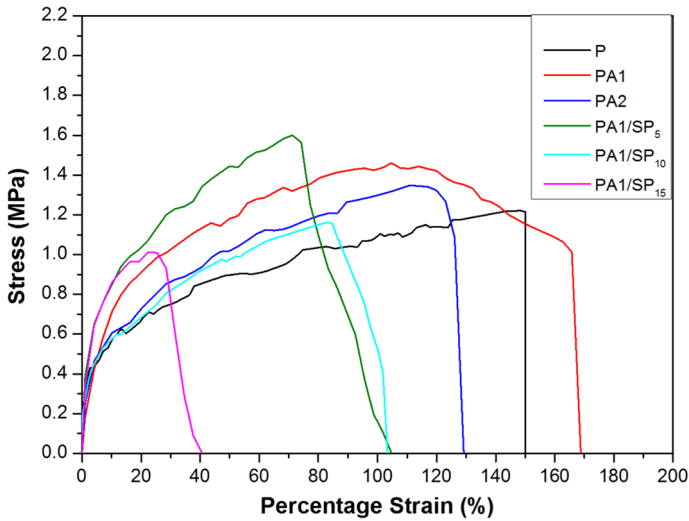


**Fig. 6** Mechanical properties of the electrospun mats

**Table 4** Mechanical properties of the electrospun mats

Sample name	Young's modulus	Tensile strength (MPa)	Elongation at break (%)
P	$2.28 \pm 2.3$	$1.21 \pm 0.38$	$158.47 \pm 16.88$
PA1	$5.17 \pm 0.99$	$1.46 \pm 0.29$	$175.15 \pm 34.61$
PA2	$2.77 \pm 0.32$	$1.34 \pm 0.46$	$129.88 \pm 8.38$
PA1/SP <sub>5</sub>	$4.38 \pm 0.15$	$1.52 \pm 0.51$	$104.4 \pm 8.60$
PA1/SP <sub>10</sub>	$1.65 \pm 0.34$	$1.13 \pm 0.13$	$103.4 \pm 2.79$
PA1/SP <sub>15</sub>	$3.77 \pm .72$	$0.93 \pm 0.17$	$40.8 \pm 3.05$

## Bioactivity

The *in vitro* hydroxyapatite formation was investigated by SEM and EDAX as shown in Fig. 7 in which PCL only fibers showed no formation of any layer. By the addition of Sr-polyP NPs, there is an obvious change in the bioactivity and the hydroxyapatite layer was confirmed by the percentage of calcium to phosphorous ratio, and it is nearly 1.67 as shown in Table 5. This is due to the bioactivity of Sr-polyP NPs which are proven to be bioactive in forming bone *in vivo* [23].

## Cytotoxicity

As shown in Fig. 8, the *in vitro* cytotoxicity assay has shown that the addition of SrPP nanoparticles has enhanced the biocompatibility of the electrospun PCL nanofibers.

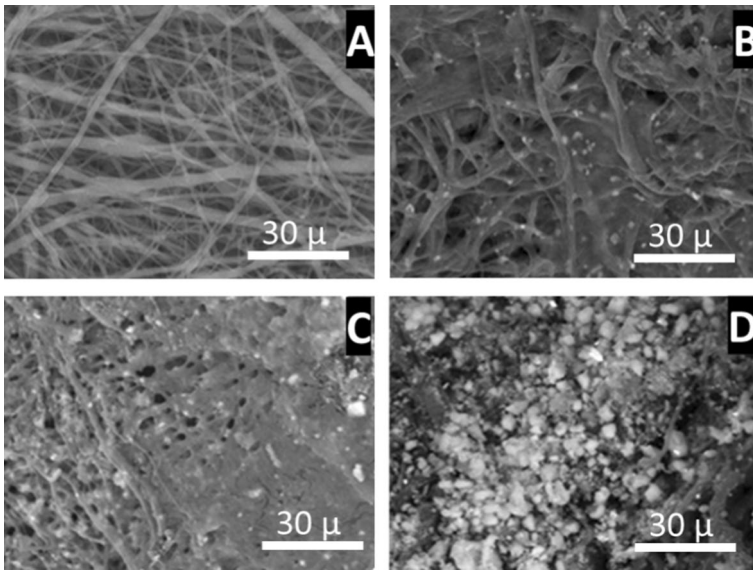


**Fig. 7** SEM of **A** P, **B** 5 PA1/SP<sub>5</sub>, **C** PA1/SP<sub>10</sub> and **D** PA1/SP<sub>15</sub>

**Table 5** Calcium and phosphorous ion ratios from EDAX

Sample	Ca	P	Ca/P
P	–	–	–
PA1/SP <sub>5</sub>	1.13	0.89	1.27
PA1/SP <sub>10</sub>	4.38	2.63	1.75
PA1/SP <sub>15</sub>	5.91	2.88	2.05

PA1/SP<sub>10</sub> has shown a significant difference compared to neat PCL; however, by increasing the Sr-polyP NPs concentration, the cytotoxicity may be due to the change in fiber morphology to be converted into a more flattened shape as shown in the SEM. The results agreed with the results obtained by Luo and his coworkers; they found that strontium addition to hydroxyapatite increased the cell viability and also the alkaline phosphatase activity [46]. Studies showed that materials containing strontium showed high angiogenesis by releasing cytokines and increased expression of physiologically active signaling molecules [47–49]. Moreover, the presence of ascorbic acid was reported to increase bone healing and has osteogenic activity as reported by Hashemi et al. [50] in their study on PLA/PCL/gelatin/ascorbic acid composite.

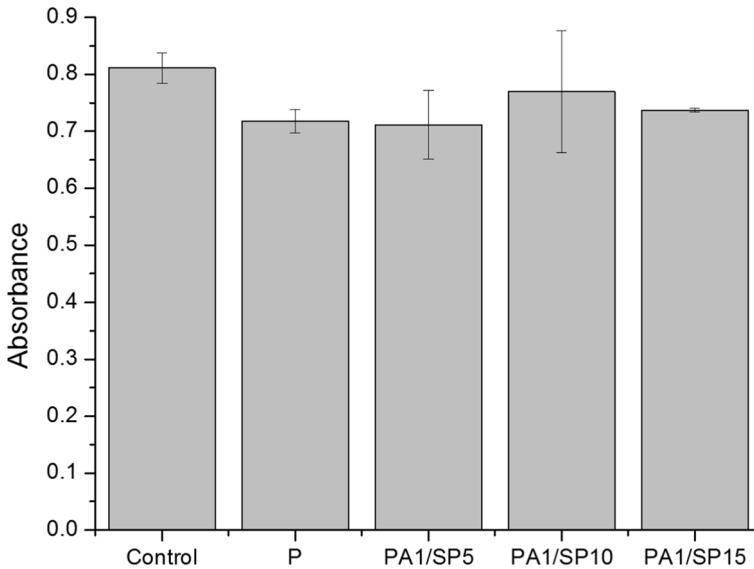


**Fig. 8** Cell proliferation assay using MTT after cell seeding on the electrospun fibers \* $p < 0.05$  indicates a significant difference between P and PA1/SP10

## Conclusions

The study deals with the electrospinning of novel antioxidant electrospun PCL/ascorbyl palmitate and the incorporation of strontium polyphosphate nanoparticles. The additives enhanced the surface wettability of PCL mats revealed leading to a high-water uptake percentage, which is of great importance for cellular attachment and proliferation. In addition, it has been proven that ascorbic acid could be released in a sustained release manner from electrospun PCL fibers under hydrolytic and enzymatic conditions. The modified electrospun mats showed higher bioactivity, mechanical properties and higher biocompatibility than pure PCL. This gives the advantage of the modified composition over the previously reported PCL mats used in bone regeneration. Therefore, obtaining such electrospun matrices loaded with multiple active compartments (i.e., AsP and Sr-polyP NPs) encourage future in vivo studies for the development of bioactive nanofibrous mats to be used in guided bone regeneration applications.

**Acknowledgements** The authors would like to thank Ahmed Gamal for his assistance in the accomplishment of this work. The paper is based upon work supported by Science and Innovation Funding Authority (STDF) and grant no. (23028).

**Funding** Open access funding provided by The Science, Technology & Innovation Funding Authority (STDF) in cooperation with The Egyptian Knowledge Bank (EKB).



## Declarations

**Conflict of interest** The authors confirm that there are no conflicts of interest.

**Open Access** This article is licensed under a Creative Commons Attribution 4.0 International License, which permits use, sharing, adaptation, distribution and reproduction in any medium or format, as long as you give appropriate credit to the original author(s) and the source, provide a link to the Creative Commons licence, and indicate if changes were made. The images or other third party material in this article are included in the article's Creative Commons licence, unless indicated otherwise in a credit line to the material. If material is not included in the article's Creative Commons licence and your intended use is not permitted by statutory regulation or exceeds the permitted use, you will need to obtain permission directly from the copyright holder. To view a copy of this licence, visit <http://creativecommons.org/licenses/by/4.0/>.

## References

1. Ye H, Zhu J, Deng D et al (2019) Enhanced osteogenesis and angiogenesis by PCL/chitosan/Sr-doped calcium phosphate electrospun nanocomposite membrane for guided bone regeneration. *J Biomater Sci Polym Ed* 30:1505–1522. <https://doi.org/10.1080/09205063.2019.1646628>
2. Elgali I, Omar O, Dahlin C, Thomsen P (2017) Guided bone regeneration: materials and biological mechanisms revisited. *Eur J Oral Sci* 125:315–337. <https://doi.org/10.1111/eos.12364>
3. Zhuang Y, Lin K, Yu H (2019) Advance of Nano-composite electrospun fibers in periodontal regeneration. *Front Chem*. <https://doi.org/10.3389/fchem.2019.00495>
4. Gentile P, Chiono V, Tonda-Turo C et al (2011) Polymeric membranes for guided bone regeneration. *Biotechnol J* 6:1187–1197. <https://doi.org/10.1002/biot.201100294>
5. Behring J, Junker R, Walboomers XF et al (2008) Toward guided tissue and bone regeneration: morphology, attachment, proliferation, and migration of cells cultured on collagen barrier membranes. *Syst Rev Odontol* 96:1–11. <https://doi.org/10.1007/s10266-008-0087-y>
6. Jung RE, Fenner N, Hämmerle CHF, Zitzmann NU (2013) Long-term outcome of implants placed with guided bone regeneration (GBR) using resorbable and non-resorbable membranes after 12–14 years. *Clin Oral Implants Res* 24:1065–1073. <https://doi.org/10.1111/j.1600-0501.2012.02522.x>
7. Veríssimo DM, Leitão RFC, Ribeiro RA et al (2010) Polyanionic collagen membranes for guided tissue regeneration: effect of progressive glutaraldehyde cross-linking on biocompatibility and degradation. *Acta Biomater* 6:4011–4018. <https://doi.org/10.1016/j.actbio.2010.04.012>
8. Berton F, Porrelli D, Di Lenarda R, Turco G (2020) A critical review on the production of electrospun nanofibres for guided bone regeneration in oral surgery. *Nanomaterials*. <https://doi.org/10.3390/nano10010016>
9. Smith LA, Ma PX (2004) Nano-fibrous scaffolds for tissue engineering. *Coll Surf B Biointerfaces* 39:125–131. <https://doi.org/10.1016/j.colsurfb.2003.12.004>
10. Niece KL, Hartgerink JD, Donners JJM, Stupp SI (2003) Self-assembly combining two bioactive peptide-amphiphile molecules into nanofibers by electrostatic attraction. *J Am Chem Soc* 125:7146–7147. <https://doi.org/10.1021/ja028215r>
11. Martin CR (1995) Template synthesis of electronically conductive polymer nanostructures. *Acc Chem Res* 28:61–68. <https://doi.org/10.1021/ar00050a002>
12. Altinkok C, Sagdic G, Daglar O et al (2023) A new strategy for direct solution electrospinning of phosphorylated poly(vinyl chloride)/polyethyleneimine blend in alcohol media. *Eur Polym J* 183:111750. <https://doi.org/10.1016/J.EURPOLYMJ.2022.111750>
13. Lian H, Meng Z (2017) Melt electrospinning vs. solution electrospinning: a comparative study of drug-loaded poly( $\epsilon$ -caprolactone) fibres. *Mater Sci Eng C* 74:117–123. <https://doi.org/10.1016/J.MSEC.2017.02.024>
14. Akay O, Altinkok C, Acik G et al (2022) Preparation of a sustainable bio-copolymer based on *Luffa cylindrica* cellulose and poly( $\epsilon$ -caprolactone) for bioplastic applications. *Int J Biol Macromol* 196:98–106. <https://doi.org/10.1016/J.IJBIOMAC.2021.12.051>

15. Ren K, Wang Y, Sun T et al (2017) Electrospun PCL/gelatin composite nanofiber structures for effective guided bone regeneration membranes. *Mater Sci Eng C* 78:324–332. <https://doi.org/10.1016/j.msec.2017.04.084>
16. Tolba E, Wang X, Ackermann M et al (2019) In situ polyphosphate nanoparticle formation in hybrid poly(vinyl alcohol)/karaya gum hydrogels: a porous scaffold inducing infiltration of mesenchymal stem cells. *Adv Sci* 6:1–15. <https://doi.org/10.1002/advs.201801452>
17. Christ JJ, Willbold S, Blank LM (2020) Methods for the analysis of polyphosphate in the life sciences. *Anal Chem* 92:4167–4176. <https://doi.org/10.1021/acs.analchem.9b05144>
18. Lorenz B, Schröder HC (2001) Mammalian intestinal alkaline phosphatase acts as highly active exopolyphosphatase. *Biochimica et Biophysica Acta (BBA) Protein Struct Mol Enzymol* 1547(2):254–261. [https://doi.org/10.1016/S0167-4838\(01\)00193-5](https://doi.org/10.1016/S0167-4838(01)00193-5)
19. Lourenço AH, Torres AL, Vasconcelos DP et al (2019) Osteogenic, anti-osteoclastogenic and immunomodulatory properties of a strontium-releasing hybrid scaffold for bone repair. *Mater Sci Eng C* 99:1289–1303. <https://doi.org/10.1016/j.msec.2019.02.053>
20. Schumacher M, Lode A, Helth A, Gelinsky M (2013) A novel strontium(II)-modified calcium phosphate bone cement stimulates human-bone-marrow-derived mesenchymal stem cell proliferation and osteogenic differentiation in vitro. *Acta Biomater* 9:9547–9557. <https://doi.org/10.1016/j.actbio.2013.07.027>
21. Lode A, Heiss C, Knapp G et al (2018) Strontium-modified premixed calcium phosphate cements for the therapy of osteoporotic bone defects. *Acta Biomater* 65:475–485. <https://doi.org/10.1016/j.actbio.2017.10.036>
22. Li S, Li L, Guo C et al (2017) A promising wound dressing material with excellent cytocompatibility and proangiogenesis action for wound healing: strontium loaded silk fibroin/sodium alginate (SF/SA) blend films. *Int J Biol Macromol* 104:969–978. <https://doi.org/10.1016/j.ijbiomac.2017.07.020>
23. Müller WEG, Tolba E, Ackermann M et al (2017) Fabrication of amorphous strontium polyphosphate microparticles that induce mineralization of bone cells in vitro and in vivo. *Acta Biomater* 50:89–101. <https://doi.org/10.1016/j.actbio.2016.12.045>
24. Mangir N, Bullock AJ, Roman S et al (2016) Production of ascorbic acid releasing biomaterials for pelvic floor repair. *Acta Biomater* 29:188–197. <https://doi.org/10.1016/j.actbio.2015.10.019>
25. Kurata SI, Senoo H, Hata RI (1993) Transcriptional activation of type I collagen genes by ascorbic acid 2-phosphate in human skin fibroblasts and Its failure in cells from a patient with  $\alpha 2(I)$ -chain-defective ehlers-danlos syndrome. *Exp Cell Res* 206:63–71. <https://doi.org/10.1006/excr.1993.1121>
26. Avizheh L, Peirouvi T, Diba K, Fathi-Azarbayjani A (2019) Electrospun wound dressing as a promising tool for the therapeutic delivery of ascorbic acid and caffeine. *Ther Deliv* 10:757–767
27. Paneva D, Manolova N, Argirova M, Rashkov I (2011) Antibacterial electrospun poly( $\epsilon$ -caprolactone)/ascorbyl palmitate nanofibrous materials. *Int J Pharm* 416:346–355. <https://doi.org/10.1016/j.ijpharm.2011.06.032>
28. Andersen FA (1999) Final report on the safety assessment of ascorbyl palmitate, ascorbyl dipalmitate, ascorbyl stearate, erythorbic acid, and sodium erythorbate. *Int J Toxicol* 18:1–26
29. Eldurini S, Abd El-Hady BM, Shafaa MW et al (2021) A multicompartement vascular implant of electrospun wintergreen oil/ polycaprolactone fibers coated with poly(ethylene oxide). *Biomed J* 44:589–597. <https://doi.org/10.1016/J.BJ.2020.04.008>
30. Müller WEG, Tolba E, Schröder HC et al (2014) Biosilica-loaded poly( $\epsilon$ -caprolactone) nanofibers mats provide a morphogenetically active surface scaffold for the growth and mineralization of the osteoclast-related SaOS-2 cells. *Biotechnol J* 9:1312–1321. <https://doi.org/10.1002/biot.201400277>
31. Ekram B, Abd El-Hady BM, El-Kady AM et al (2021) Enhanced mesenchymal stem cells growth on antibacterial microgrooved electrospun zinc chloride/polycaprolactone conduits for peripheral nerve regeneration. *J Bioact Compat Polym*. <https://doi.org/10.1177/0883911520988305>
32. Sobh R, Mohamed W, Ekram B (2019) Fabrication of acrylic modified surface of polyamide 6/CaO electrospun nanofibrous membrane for effective dye removal. *Egypt J Chem* 0(0):0–0. <https://doi.org/10.21608/ejchem.2019.19498.2187>
33. Schneider CA, Rasband WS, Eliceiri KW (2012) NIH image to imageJ: 25 years of image analysis. *Nat Methods* 9:671. <https://doi.org/10.1038/NMETH.2089>
34. Plank D, Valley H, Wonderful POM, et al (2012) Determination of antioxidant activity in foods and beverages by reaction with 2,2'-Diphenyl-1-picrylhydrazyl (DPPH): collaborative study first action 2012.04. *J AOAC Int* 96:1562–1569. [https://doi.org/10.5740/jaoacint.CS2012\\_04](https://doi.org/10.5740/jaoacint.CS2012_04)

35. Deyab NM, Ekram B, Badr KR et al (2022) Antiviral electrospun polyamide three-layered mask filter containing metal oxide nanoparticles and black seed oil. *ACS Omega* 7:44438–44447. [https://doi.org/10.1021/ACSEMEGA.2C06611/ASSET/IMAGES/LARGE/AO2C06611\\_0008.JPEG](https://doi.org/10.1021/ACSEMEGA.2C06611/ASSET/IMAGES/LARGE/AO2C06611_0008.JPEG)
36. Kandil H, Ekram B, Abo-Zeid MAM (2022) Cytocompatibility of MG-63 osteosarcoma cells on chitosan/hydroxyapatite/lignin hybrid composite scaffold in vitro. *Biomed Mater* 18:015002. <https://doi.org/10.1088/1748-605X/AC9F92>
37. Avizheh L, Peirouvi T, Diba K, Fathi-Azarbayjani A (2019) Electrospun wound dressing as a promising tool for the therapeutic delivery of ascorbic acid and caffeine. *Therapeutic Deliv* 10:757–767. <https://doi.org/10.4155/TDE-2019-0059>
38. Hassan MI, Sultana N, Hamdan S (2014) Bioactivity assessment of poly ( $\epsilon$ -caprolactone)/hydroxyapatite electrospun fibers for bone tissue engineering application. *J Nanomater*. <https://doi.org/10.1155/2014/573238>
39. Deliormanli AM (2015) Preparation and in vitro characterization of electrospun 45S5 bioactive glass nanofibers. *Ceram Int* 41:417–425. <https://doi.org/10.1016/J.CERAMINT.2014.08.086>
40. Wiens M, Wang X, Schlomacher U et al (2010) Osteogenic potential of biosilica on human osteoblast-like (SaOS-2) cells. *Calcif Tissue Int* 87:513–524. <https://doi.org/10.1007/s00223-010-9408-6>
41. Du L, Xu HZ, Li T et al (2017) Fabrication of ascorbyl palmitate loaded poly(caprolactone)/silver nanoparticle embedded poly(vinyl alcohol) hybrid nanofibre mats as active wound dressings: Via dual-spinneret electrospinning. *RSC Adv* 7:31310–31318. <https://doi.org/10.1039/c7ra03193a>
42. Bayrak E, Ozcan B, Erisken C (2016) Processing of polycaprolactone and hydroxyapatite to fabricate graded electrospun composites for tendon-bone interface regeneration. *J Polym Eng* 37:99–106. <https://doi.org/10.1515/polyeng-2016-0017>
43. Díaz E, Sandonis I, Valle MB (2014) In vitro degradation of poly(caprolactone)/nHA composites. *J Nanomater*. <https://doi.org/10.1155/2014/802435>
44. Sánchez-Moreno C, Larrauri JA, Saura-Calixto F (1998) A procedure to measure the antiradical efficiency of polyphenols. *J Sci Food Agric* 76:270–276. [https://doi.org/10.1002/\(SICI\)1097-0010\(199802\)76:2%3c270::AID-JSFA945%3e3.0.CO;2-9](https://doi.org/10.1002/(SICI)1097-0010(199802)76:2%3c270::AID-JSFA945%3e3.0.CO;2-9)
45. Rivero-Cruz JF, Granados-Pineda J, Pedraza-Chaverri J et al (2020) Phytochemical constituents, antioxidant, cytotoxic, and antimicrobial activities of the ethanolic extract of mexican brown propolis. *Antioxidants*. <https://doi.org/10.3390/antiox9010070>
46. Luo Y, Chen S, Shi Y, Ma J (2018) 3D printing of strontium-doped hydroxyapatite based composite scaffolds for repairing critical-sized rabbit calvarial defects. *Biomed Mater* 13:065004. <https://doi.org/10.1088/1748-605X/AAD923>
47. Mao L, Xia L, Chang J et al (2017) The synergistic effects of Sr and Si bioactive ions on osteogenesis, osteoclastogenesis and angiogenesis for osteoporotic bone regeneration. *Acta Biomater* 61:217–232. <https://doi.org/10.1016/j.actbio.2017.08.015>
48. Neves N, Linhares D, Costa G et al (2017) In vivo and clinical application of strontium-enriched biomaterials for bone regeneration: a systematic review. *Bone Joint Res* 6:366–375. <https://doi.org/10.1302/2046-3758.66.BJR-2016-0311.R1>
49. Yan MD, Ou YJ, Lin YJ et al (2022) Does the incorporation of strontium into calcium phosphate improve bone repair? A meta-analysis. *BMC Oral Health* 22:1–21. <https://doi.org/10.1186/S12903-022-02092-7/FIGURES/7>
50. Hashemi SF, Mehrabi M, Ehterami A et al (2021) In-vitro and in-vivo studies of PLA / PCL / gelatin composite scaffold containing ascorbic acid for bone regeneration. *J Drug Deliv Sci Technol* 61:102077. <https://doi.org/10.1016/J.JDDST.2020.102077>

## Authors and Affiliations

**Bothaina M. Abdel-Hady<sup>1</sup> · Basma Ekram<sup>1</sup>  · Werner E. G. Müller<sup>2</sup> · Abdul Aziz M. Gad<sup>3</sup> · Xiaohong Wang<sup>2</sup> · Heinz C. Schröder<sup>2</sup> · Emad Tolba<sup>1</sup>**

✉ Basma Ekram  
basmaekram@yahoo.com

✉ Emad Tolba  
emad\_nrc@yahoo.com

<sup>1</sup> Polymers and Pigments Department, National Research Centre, Chemical Industries Research Institute, Dokki, Cairo 12622, Egypt

<sup>2</sup> ERC Advanced Investigator Grant Research Group at the Institute for Physiological Chemistry, University Medical Center of the Johannes Gutenberg University, Duesbergweg 6, 55128 Mainz, Germany

<sup>3</sup> Molecular Biology Department, National Research Centre, Biotechnology Research Institute, Dokki, Cairo 12622, Egypt